IEEE Access
Multidisciplinary | Rapid Review | Open Access Journal

Received February 12, 2021, accepted February 20, 2021, date of publication February 23, 2021, date of current version March 4, 2021.

Digital Object Identifier 10.1109/ACCESS.2021.3061640

Ten Antenna Array Using a Small Footprint Capacitive-Coupled-Shorted Loop Antenna for 3.5 GHz 5G Smartphone Applications

SAQER S. ALJA'AFREH[1], BAYAN ALTARAWNEH[1], MALLAK H. ALSHAMAILEH[1], E'QAB R. ALMAJALI[2], RIFAQAT HUSSAIN[3], MOHAMMAD S. SHARAWI[4], (Senior Member, IEEE), LEI XING[5], (Member, IEEE), AND QIAN XU[5], (Member, IEEE)

[1]Electrical Engineering Department, Mutah University, Mu'tah 61710, Jordan
[2]Electrical and Computer Engineering Department, University of Sharjah, Sharjah 27272, United Arab Emirates
[3]Electrical Engineering Department, King Fahd University of Petroleum & Minerals, Dhahran 31261, Saudi Arabia
[4]Electrical Engineering, Department, Polytechnique Montréal, Montreal, QC H3T 1J4, Canada
[5]College of Electronic and Information Engineering, Nanjing University of Aeronautics and Astronautics, Nanjing 210016, China

Corresponding author: Saqer S. Alja'afreh (saqer1981@yahoo.com)

This work was supported in part by Mutah University, Jordan, and in part by King Fahd University of Petroleum and Minerals (KFUPM), Saudi Arabia.

ABSTRACT A self-isolated 10-element antenna array operating in the long-term evolution 42 (LTE42) frequency band is proposed for 5G massive MIMO smartphone applications. The proposed antenna elements are placed in a 2D array configuration; they are placed symmetrically along the two long edges of the mobile chassis. The proposed antenna structure is a shorted loop antenna resonating at half-wavelength mode, which is rarely deployed by researchers due to its large size compared to other quarter wavelength antenna structures. It is a printed, shorted, and compact loop antenna of a total footprint area of 6×6.5 mm^2 ($\lambda/14.3 \times \lambda/13.2$, where λ is the free space wavelength at 3.5 GHz). A small capacitive coupling flag-shaped strip is used to excite the proposed loop antenna. The compactness is achieved using an inward meandering that forms an internal loop in the element. The position and the dimensions of this loop are used to tune the resonant frequency and matching level at 3.5 GHz. The results (theoretical, simulated, and measured) show that the 3.5 GHz band (3.4-3.6 GHz) is achieved with impedance matching better than -10 dB, and total efficiency higher than 65%. A 10×10 MIMO system is formed and it has an excellent MIMO and diversity performance in-terms of the envelope correlation coefficient (below 0.055), and apparently it has the highest channel capacity (about 54.3 bps/Hz) among other MIMO systems of the same order. Simulation results of the specific absorption rate (SAR) demonstrates that the proposed antenna solution satisfied SAR criterion. Thus, the proposed ten-element MIMO antenna represent an excellent candidate for sub-6 GHz 5G smartphone applications.

INDEX TERMS 5G antennas, loop antennas, sub-6 GHz antennas, smartphone antennas.

I. INTRODUCTION

The 5G communications system represents one of the latest wireless solutions as it offers a high data rate with very low latency. In release 15 of the 3GPP, two major NR 5G frequency bands were defined: Frequency band 1 (FR1, 450-6000 MHz) and frequency band 2 (FR2, 24.25-52.6 GHz) [1], [2]. Several sub-bands are included in these two bands. The sub-6 GHz band (3.4-3.6) represents one of the well-known bands that receive a huge interest from researchers [3]–[22].

In order to achieve the main themes of 5G communication systems (very high data rate, very low latency), massive multiple inputs and multiple outputs (mMIMO) antenna should be carefully designed at both communications end (the base station and the mobile station). Due to the limited space, the design of the MIMO antenna system for hand-portable devices is quite

The associate editor coordinating the review of this manuscript and approving it for publication was Mohammad Tariqul Islam.

challenging for antennas' engineers in both industry and academia [23].

The current state-of-the-art of sub-6 5G smartphone mMIMO antennas can be classified based on four aspects; *(1)* Mode of operation; single-band antennas [3]–[7], [15], [16], [19], dual-band antennas[11], [17], [21], and wideband antennas [10], [12], [20]. *(2)* The number of antenna elements; it has been proposed that the promising number of antenna elements for 5G mMIMO operation should be at least eight [3]. Therefore, numerous published works reported 8-element MIMO antenna array [3]–[7], [9], [10], [12], [16], [17], [20], and [21]. However, a few works consider 5G antenna composed of 10 elements and more [14], [15], and [18]. *(3)* The use of isolation circuitry; several designs have utilized decoupling techniques such as: neutralization line [16], [18], [22], parasitic elements [17], [21], antenna elements arrangement [9], [10], [16], [18], [20], polarization diversity [7]–[9], and self-isolated antennas [4]–[6], [11]. However, among all of these, antennas having self-isolation represent a promising solution due to the simplicity of the overall antenna circuit [11]. *(4)* Antenna structure; the current-state-of-the-art includes two practical implementation choices for the installation of 5G antennas in smartphones: the face–antenna design, and the edge-antenna design [24]. The very well-known one is the edge-antenna design, in which antenna elements are normally placed on the edges, which normally represents the metal frame of the device. Therefore, most of the published 5G sub-6 GHz antennas are built as a part of the metal frame of smartphone devices [3], [8], [13], [15], [16], [22]. In this regard, different antenna structures have been proposed such as: inverted-F antennas (IFA) [12], [18], dipole-like antennas [11], [19], split loop [17], slot monopoles [14], [15], [20], monopoles [3], [4], [9], [21], open slot on bezel [7], and inverted-L antennas [25], [26].

Dual-element compact building blocks, like those reported in [6], [27], represent a promising approach in developing massive MIMO antenna arrays. However, despite the huge number of elements that can be used, these designs are believed to fail in presenting the effect of a user's hand on the total radiation efficiency. This simply occurs because a user hand can cover many elements at once due to such elements grouping. To the best of our knowledge, the single element approach represents an effective approach, especially, if the building element does not include a big gap like the shorted loop structure we propose. Such a structure does not attract researchers' attention as other structures like monopole, slot monopole and slot antennas as these latter structures have fundamental resonating radiating modes at about a quarter wavelength. This encouraged researchers to use these antenna types in order to ensure the best utilization of the limited space inside a smartphone. Additionally, the design of dual-band [11], [17], wideband [10], [12] antennas is very simple using these structures. Actually, very few works used loop antennas [5], [6], [11], [19] for smartphones since loop antennas normally have half-wavelength fundamental mode, and hence their physical size normally greater than other antenna structures.

Surprisingly, most researchers have overlooked the use of loop antennas for 5G sub-6 GHz applications but only very few works developed loop-type antennas [5], [6], [8]; loop antenna structures normally have a matching problem and a narrowband impedance bandwidth. However, Loop antennas have very important features such as: *1)* high detuning resistance (insensitive to hand and head touch events), and the low specific abortion rate (SAR) [28]. Normally, other antenna structures are electric field antennas like PIFA, monopoles, slot monopoles, bezel gap antennas. They normally have a high electric field in the near-field region, which in-turns result in high SAR and high detuning due to the user's hand. Unlike electric field-based antennas, loop antennas and electrically coupled loop antennas are magnetic field antennas that have a high magnetic field in the near field. Thus, their SAR and detuning are negligible compared to the electric field ones. *2)* Grounded loop antennas normally have symmetrical current mode [29]. This gives an extra advantage of the resulted loop antenna arrays. They are normally uniform antenna arrays having identical antenna elements with equal spacing (highly recommended for cost effective corporate feeding networks in 5G antenna arrays. [30]. Such unique property cannot be achieved using antenna structures that have a non-symmetrical current mode (monopole, slot monopole and IFA) [31]. *3)* The lowest and fundamental resonance mode of the grounded loop antenna structures is $\lambda/2$ mode. Based on image theory, such loop structure is equivalent to conventional one wavelength loop antenna. Therefore, grounded loop antenna of $\lambda/2$ resonance mode represents a large loop antenna that have an antenna gain greater than other structures like monopole, slot monopole and slot antennas [32]. Overall, loop antennas represent a promising antenna structure for edge-build sub-6 GHz 5G smartphone antennas.

This article is organized as follows: Section II presents the proposed 10-element antenna system, the antenna element structure, and the design considerations. Section III addresses the design evolution process, the equivalent lumped circuit model of the antenna structure, and the performed parametric study. The MIMO performance and other antenna radiation characteristics are presented in Section IV through both the simulated and measured results. Section V summarizes the current state-of-the-art with respect to the proposed work. Finally, Section VI concludes the article.

II. THE PROPOSED ANTENNA SYSTEM

In this section, the geometry of the proposed 10-element MIMO antenna array for 5G smartphone applications is presented first, and then the structure of the proposed antenna-element is discussed in detail.

A. THE PROPOSED MIMO ARRAY

The geometry of the proposed 10-element antenna is illustrated in Fig. 1. It comprises of ten identical

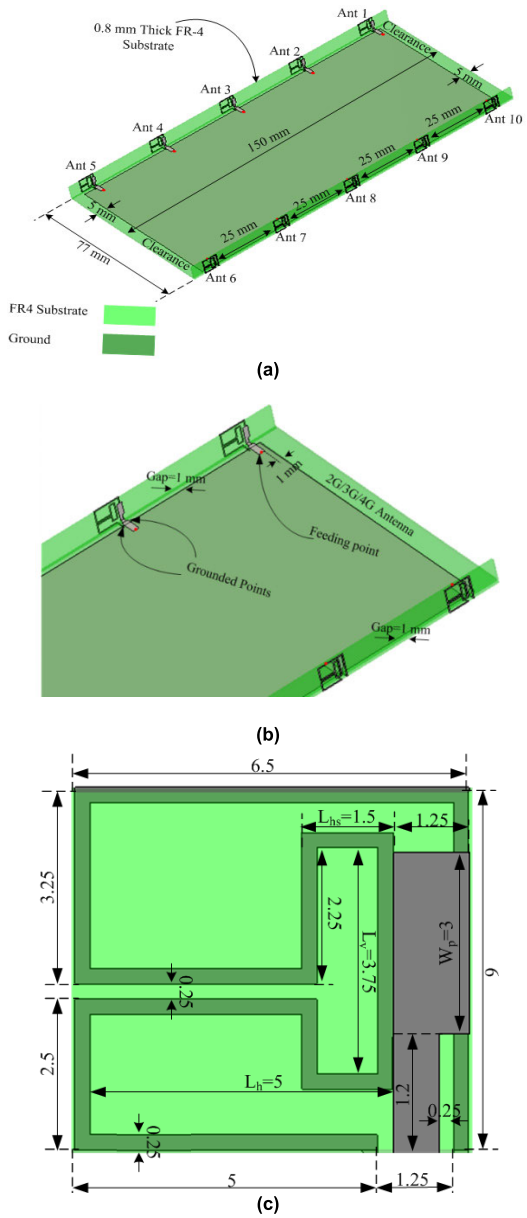

FIGURE 1. The perspective of the proposed antenna design. (a) Perspective view; (b) Zoomed in view (c) Detailed dimensions of the proposed antenna element. [units are in mm].

capacitive-coupled loop antenna elements, which are printed on two double-sided FR4 substrates, each one of dimensions $150 \times 6 \times 0.8$ mm^3 and are placed along the two long edges of the mobile circuit board. A 0.8 mm thick FR4 ($\varepsilon_r = 4.3$, $\tan\delta = 0.02$) is used as a system circuit board of dimensions 150×77 mm^2, which is typical for 5.5-inches Smartphones. The substrate has two clearance areas, each one of a size of 5×77 mm^2 at both the bottom and top edges of the system ground plane. These two regions are typically reserved for 4G, 3G, and 2G and for MIMO antennas (main and diversity antennas). It is worth mentioning that the size of clearance regions can be further decreased without affecting the performance of the proposed 5G massive MIMO antennas.

The 10-element antenna is printed on the external sides of the two small substrates; each substrate has five antenna elements. As shown closely in Fig.1(b), a 1 mm gap is created between the ground plane and both edges (small substrates). Each antenna element is excited through a capacitive-coupled feed (feeding plate). This feeding plate is connected to a 50 Ω microstrip feed line while the microstrip feed line is coupled through a 50 Ω SMA connector through a via-hole from the backside of the system PCB board. The SMA connectors are not shown in the proposed configuration for the purpose of brevity. As depicted by Fig.1(c), the proposed antenna element is a grounded loop structure. The edge-to-edge distance between any two adjacent elements is about 25 mm on each long-edge side (the small substrates).

B. THE PROPOSED ELEMENT STRUCTURE

The detailed geometry and dimensions of the proposed antenna element are shown in Fig. 1(c). The structure represents a grounded loop-type antenna. It consists of two parts, namely; a small coupling flag-shaped feeding plate, and a very small printed loop of dimensions 6×6.5 mm^2 ($0.07\lambda \times 0.0758\lambda$, where λ is the free space wavelength at 3.5 GHz). To improve the antenna effective volume (size), the loop antenna is meandered inward to make an internal sub-loop inside. The position and the dimensions of the internal loop are used to tune the resonant frequency and the matching level at 3.5 GHz. Therefore, the proposed antenna is fundamentally resonant with a half-wavelength loop mode at 3.5 GHz to cover LTE band 42 (3400-3600) based on the −10 dB bandwidth criterion.

III. DESIGN EVOLUTION PROCESS, EQUIVALENT CIRCUIT MODEL AND PARAMETRIC STUDY

In this Section, an evolutional design process of the proposed basic antenna element will be demonstrated. Then, an equivalent circuit model is proposed for a better understanding of the theory behind the designed antenna element. Finally, a parametric study for some of the vital design parameters is presented in order to further illustrate the working principle of the proposed antenna element.

A. ANTENNA ELEMENT DESIGN PROCESS

The design process starts with a conventional simple rectangular loop (REF1) that is shorted to the ground plane as shown in Fig. 2(a). As is seen in Fig. 2(a), a capacitive coupling feed is deployed to excite a half wavelength loop mode around 3.5 GHz band. By doing so, the structure resonates in its half-wavelength mode. This can be seen from the surface current distribution at 3.5 GHz that is shown in Fig. 3(a). Additionally, it shows a null current location (half-wavelength loop mode) on the upper arm of the loop antenna. This represents an interesting finding; at such location, the loop can be meandered/folded/bent in any way with minimal effects on the current distribution [33].

Therefore, the next logical step is to bend/meander the loop in its plane (internal fold). This allows more reduction in the antenna size while resonating at the same frequency band of interest. However, to gain more from such a meandering

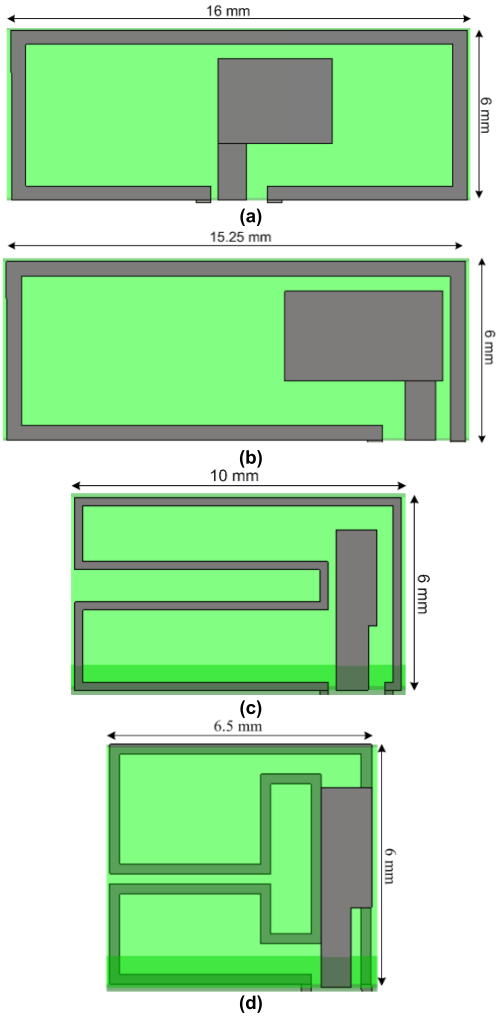

FIGURE 2. Structure geometry description to stages of reducing the size of the proposed antenna (a) REF1 .(b) REF2. (C) REF3. (d) REF4.

process, the location of the null current point (in Fig. 3(a)) should be moved from the top of the loop to one of its vertical sides. This can be done by shifting the feed position toward the side edges as shown in the REF2 antenna exhibited in Fig. 2(b). However, by doing the said feed location change, the matching level around 3.5 GHz has deteriorated as revealed by the reflection coefficient results shown in Fig. 4. Despite that, the feed point shift produced the interesting outcome shown in Fig. 3(b) whereby a new location for the current null is now created on the left side of the loop antenna. In order to improve the deteriorated matching level, a horizontal meandered section is created as shown in Fig. 2(c) (REF3). This from one side reduced the total dimensions of the loop to 10×6 mm^2 and enhanced the matching level around 3.5 GHz significantly as shown in Fig. 4.

In order to save more space and to enhance the total impedance bandwidth, an internal small loop has been also created at the end of the loop as shown in Fig. 2(d) (REF4, which represents the proposed antenna structure in this article). This new vertical fold led to an increase of the capacitive

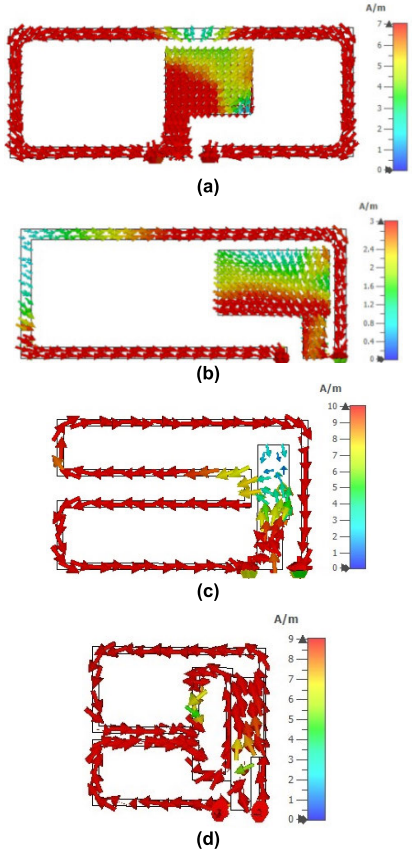

FIGURE 3. Simulated current distributions at 3.5 GHz (a) REF1. (b) REF2. (c) REF3 and (d) REF4.

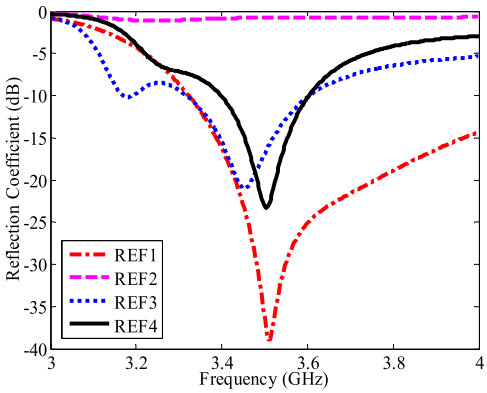

FIGURE 4. Evolution of the reflection parameter.

coupling between the feed and the loop over the entire operational bandwidth. This created a reasonable operational bandwidth centered around 3.5 GHz, based on the -10 dB criterion, to cover the whole LTE42 band (3400-3600 MHz) as shown in Fig. 4. Another advantage of the latter geometry change is the size reduction associated with it; the total size eventually is decreased to be only 6.5×6 mm^2. The total length of the resulted loop antenna is about 40.5 mm, which is close to one-half wavelength at 3500 MHz. The current distribution shown in Fig. 3(d) ties very well with the mentioned

TABLE 1. Size Reduction Percentage and Maximum Number of Elements After Each Step in the Design Process.

Structure geometry	Area (mm^2)	Size reduction percentage	Max # of elements
REF1	96	00.0%	3×2=6
REF2	91.5	4.68%	3×2=6
REF3	60	37.5%	4×2=8
REF4	39	59.37%	5×2=10

dimension as the excited current mode is a half wavelength mode at 3.5 GHz.

Table 1 summarizes the design process and highlights the big advantage of the proposed antenna block. It shows how much percentage in size reduction after every single step of the design process achieved compared to the initial design size. The final design size is 59.37% smaller than the initial design structure without using any lumped elements' or matching circuits. The significant reduction of the element size has allowed for a sufficient space to include10 elements instead of 6 or 8 along both edges of the smartphone, as illustrated by other designs reported in the open literature, while maintaining acceptable values for both the antenna efficiency and the isolation level as will be illustrated later, assuming the same separation distance about 25 mm.

B. EQUIVALENT LUMPED CIRCUIT MODEL

To understand the theory and the true behavior of the proposed antenna structure, an equivalent lumped circuit model is developed for any two adjacent antenna elements in the proposed antenna array. Ant 2 and Ant 3 are considered here to elaborate on the mutual coupling effect. The following steps summaries the development process of the equivalent circuit model with mutual coupling incorporation:

1. The feeding strip excites the antenna element through capacitive coupling. This is shown in Fig. 5(a). The results shown in Fig. 4 reveal clearly that the best matching level is achieved when the capacitive feed strip is placed in the middle of the loop structure (half loop to the right of the feeding strip, while the second half is to the left). The surface current distributions shown in Fig. 3 confirms that as the feeding strip should have better excitation when it is located at a null current location (normally at the middle of the loop structure).
2. Each half of the loop, shown in Fig. 5(a), represents a short-circuited transmission line resonator. Therefore, the general configuration of the antenna structure looks like a two parallel short-circuited transmission line resonators that are excited by the feeding strip. In order to show the two short circuited transmission lines clearly, the equivalent circuit of the antenna element port, the feeding strip, and the coupling capacitances is drawn first as shown in Fig. 5(b). The antenna element port is modeled as 50 Ω voltage source $\boldsymbol{V_g}$. The small feeding strip is replaced by a series resistance $\boldsymbol{R_s}$ and a series inductance $\boldsymbol{L_s}$. The capacitor $\boldsymbol{C_g}$ is due to coupling between antenna structure and the ground plane, while the gap between the feeding strip and the loop is represented by the capacitance $\boldsymbol{C_c}$.
3. As the length of each half is around a quarter wavelength, the normal lumped circuit model for it is a parallel RLC resonance circuit shown in Fig. 5(c). $\boldsymbol{R_a}$, $\boldsymbol{C_a}$, and $\boldsymbol{L_a}$ represent the total equivalent circuit elements of the two parallel RLC circuits [34]. Over all, a single element loop structure can be modeled as a parallel resonance RLC circuit fed by an L-shaped feeding and matching circuit as shown in Fig. 5(c).

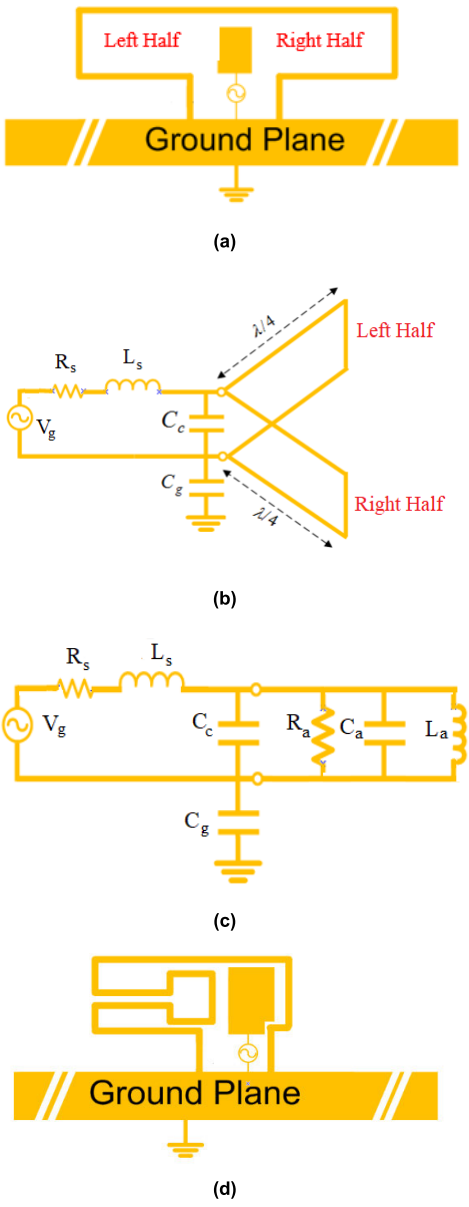

FIGURE 5. Equivalent circuit model of isolated antenna element, (a) REF 1 antenna to clarify the symmetry of the feed location, (b) Equivalent circuit of the feeding strip, (c) Lumped equivalent circuit model of the optimized structure and (d) Optimized antenna structure. Circuit elements values are: $R_s = 9\Omega$, $L_s = 7.4$ nH, $C_c = 1$ PF, $L_a = 1.257$ nH, $C_a = 2$ PF, $R_a = 250$ Ohm, $C_g = 0.75$ PF.

4. Mutual coupling circuit modeling: The results of mutual coupling coefficients shows, as expected, that the highest mutual coupling level occurs between adjacent antenna elements. Therefore, we here consider studying the coupling between two adjacent antenna namely, Ant 2 and Ant 3 shown in Fig. 1(a). The same principle and circuitry is also valid for every two adjacent elements in the proposed antenna array. In [35], a very powerful coupling circuit model is presented for densely packed arrays with element separation of less than half wavelength. They compensate the problem of mutual coupling among multi-feed antennas by using proper filtering functions [35], [36]. Consequently, the combination of any two adjacent antenna elements (like Ant 2 and Ant 3 we consider here) are loosely coupled to feeding ports. The coupling coefficient can then be extracted from the mutual coupling coefficient curves (S_{32} & S_{23} as shown in Fig. 6(a)). The two resonance peaks $\boldsymbol{f_1}$ and $\boldsymbol{f_2}$ deternt $\mathbf{K_{23}}$ as described by (1) [34]:

$$K_{23} = \frac{f_2^2 - f_1^2}{f_2^2 + f_1^2} = \frac{(3.415)^2 - (3.3)^2}{(3.415)^2 + (3.3)^2} = 0.035 \quad (1)$$

5. The mutual coupling coefficient will lead to find the mutual inductance between coupled loop circuits. The mutual inductance is normally defined as a multiplication of the mutual coupling coefficient and the square root of self-inductances product as described by (2) [37]. In this regard, Fig. 6(b) shows the equivalent circuit of Ant 2 and Ant 3 coupled through a transformer coupling. Based on the circuit theory of magnetically coupled circuits in [36], the transformer coupling in Fig. 6(b) can be replaced by an equivalent T-network as depicted in Fig. 6(c). Equation (3) and (4) are used to find the T-network element's values [36]. It is worth mentioning that the values of $\boldsymbol{L_1}$ and $\boldsymbol{L_2}$ are equal as $\boldsymbol{L_a}$ and $\boldsymbol{L_b}$ due to the reciprocity of the S_{23} and S_{32} curves. Overall. Fig. 6(a) shows that the proposed circuit model generates scattering parameters that are very similar to the extracted ones from the 3D full-wave CST model.

$$M_{23} = K_{12}\sqrt{L_a L_b} \quad (2)$$

$$L_1 = L_a - M_{23} \quad (3)$$

$$L_2 = L_b - M_{23} \quad (4)$$

C. PARAMETRIC STUDY

A parametric study of vital design parameters led to a better understanding of the achieved results and the working mechanism of the proposed antenna. The study is conducted using CST Microwave Studio. The parameter of interest is changed, while other design parameters are kept constant. In this study, the effects of four important design parameters are investigated. These parameters are: the position of the feed, the horizontal meandered length (L_h),

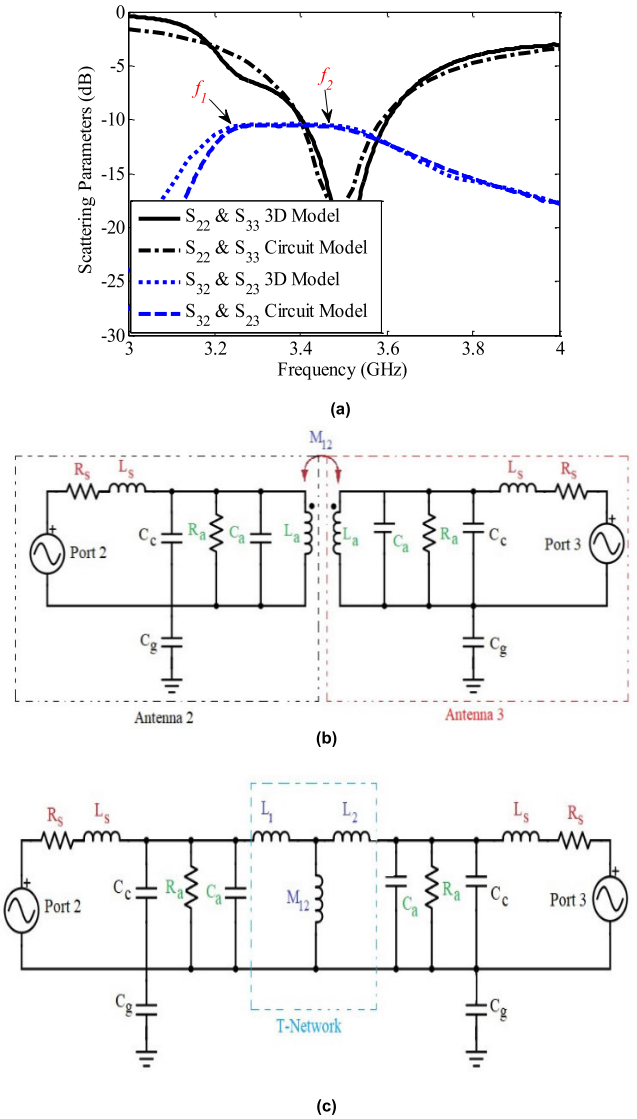

FIGURE 6. Equivalent circuit of two adjacent antenna elements: Ant 2 and Ant 3 are considered. (a) Scattering parameters of both circuit and 3D models. (b) Two individual antennas circuits coupled through a mutual inductance, $M_{12} = 0.072$ nH. (c) Over all equivalent circuit model of Ant 2 and Ant 3, $M_{12} = 0.072$ nH, $L_1 = L_2 = 1.23$ nH.

the small horizontal meandered length (L_{hs}), and finally, the vertical length of the inner loop (vertical meandered length) (L_v). As all antenna elements are identical, Fig. 7, Fig. 8, Fig. 9, and Fig. 10 present only the reflection coefficient response of element 3 in the proposed massive MIMO array.

Fig. 7. shows the feed position effect on the level of matching and the operational bandwidth. It is evident that such a parameter plays an important role in determining the level of matching and the operational bandwidth. Accordingly, it was observed that the best location for the feed point is close to the right edge of the proposed loop as shown in Fig. 2. At this location, the maximum capacitive coupling occurs between the loop and the feeding plate (the capacitive feed is very near to the null current point). In order to optimize the −10 dB

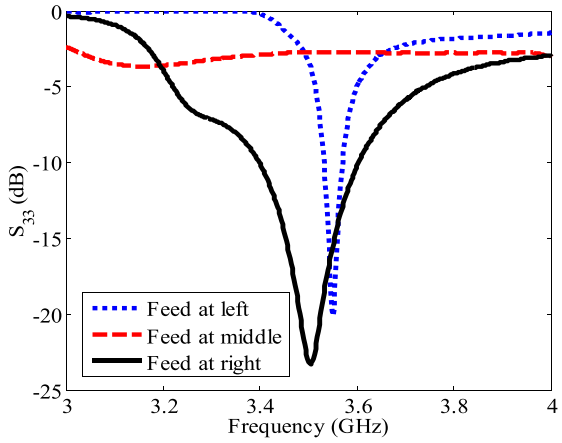

FIGURE 7. Simulated S_{33} with different feed position.

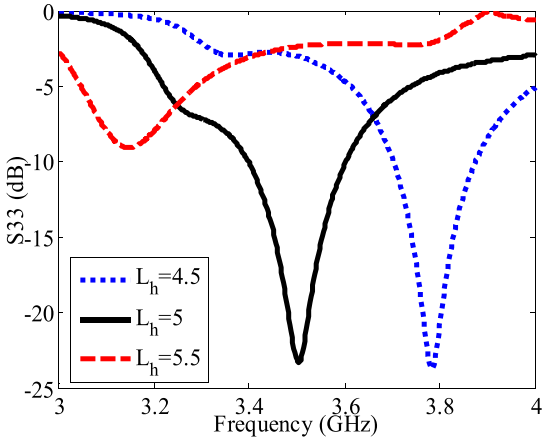

FIGURE 8. Simulated S_{33} with different L_h.

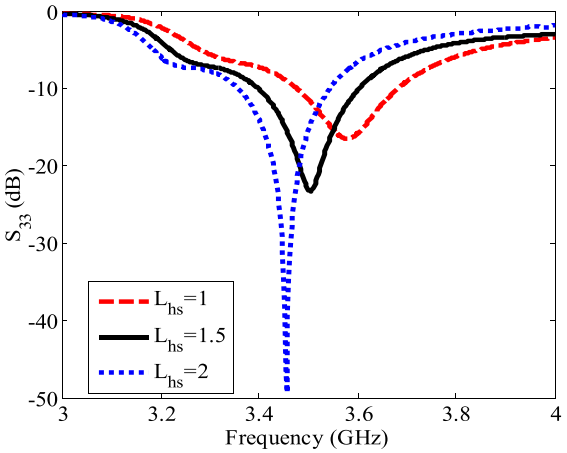

FIGURE 9. Simulated S_{33} with different L_{hs}.

impedance bandwidth in the desired frequency band, the right location was chosen.

Fig. 8. shows that the simulated reflection coefficient is highly affected by the horizontal meandered length (L_h). The variation of L_h does not affect only the resonant frequency, it also affects the level of matching. More clearly, as L_h decreases, the resonant frequency increases, and the operational bandwidth is shifted upward in the frequency band. This is expected as it affects the total length of the proposed loop antenna. $L_h = 5$ mm is selected so that the optimum 10 dB return loss impedance bandwidth is achieved in the desired frequency band.

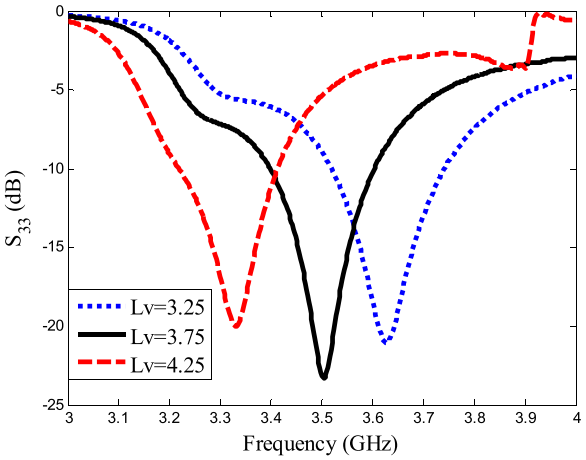

FIGURE 10. Simulated S_{33} with different L_v.

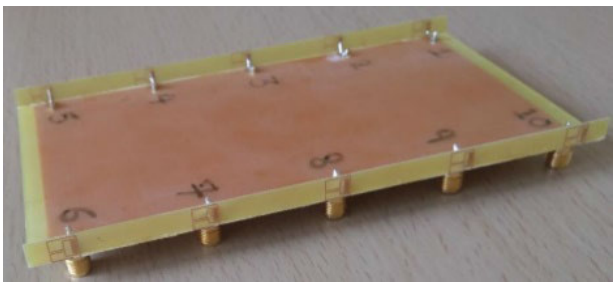

FIGURE 11. Proposed antenna prototype.

Another effective parameter is the small horizontal meandered length which has been symbolized L_{hs} in Fig. 1(c). The reflection coefficient is simulated for different small horizontal meandered lengths and the results are shown in Fig. 9. It is found that by increasing the small horizontal meandered length, the resonant frequency is shifted downward in the frequency band. The level of the matching increases decently. $L_{hs} = 1.5$ mm is selected in order to maintain the coverage of the 3.4 - 3.6 MHz band for an optimum 10 dB return loss impedance.

In a similar manner, Fig. 10 shows that changing the vertical length of the inner loop will tune to the resonant length of the proposed antenna element so that it affects the resonant frequency of interest. $L_v = 3.75$ mm is selected so that the optimum 10 dB return loss impedance bandwidth is achieved in the desired frequency band.

IV. SIMULATED AND MEASURED RESULTS OF THE PROPOSED ANTENNA

In this Section, important simulated results are validated through the measured results of a fabricated prototype antenna, which is attached to Fig. 11. First, the scattering

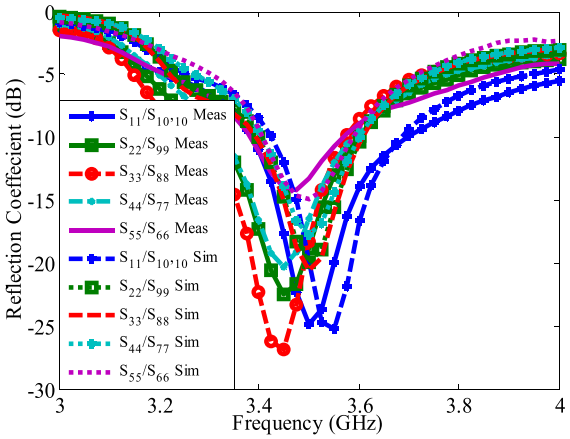

FIGURE 12. Simulated and measured reflection parameters.

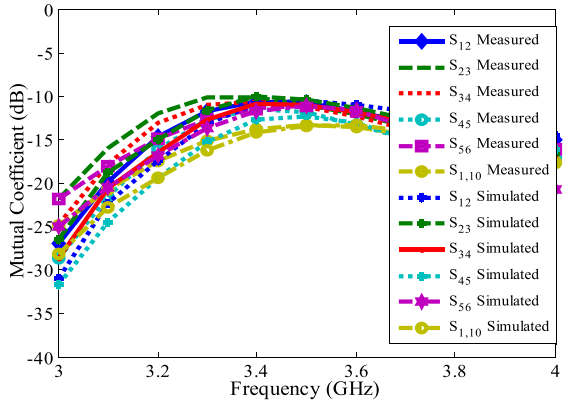

FIGURE 13. Simulated and measured mutual coupling coefficients results.

parameters are presented and discussed. After that, the radiation characteristics in-terms of the simulated radiation patterns and the total radiation efficiencies are explained. Then, important MIMO performance parameters like ECC is calculated and presented. Finally, the user's hand effect is investigated and compared with the state of the art.

A. SCATTERING PARAMETERS

The simulated and measured results of the reflection coefficients are shown in Fig. 12. One can observe that both simulated and measured results are in good agreement. Additionally, all the proposed antenna elements are proved to cover the whole sub-6 GHz band namely LTE42 (3400-3600 MHz) based on a 10 dB return loss criterion. It is evident from Fig. 12 that each element on the right side has a similar reflection coefficient to its corresponding element on the left side.

Fig. 13 shows the simulated and measured mutual coupling parameters between the different antenna elements of the proposed 10-element antenna array. Because the array is symmetrically placed, some isolation curves are better than 12 dB over the entire frequency band of interest. Only six curves are presented, which are the ones for the adjacent antenna elements as they have the strongest coupling level. Generally speaking, the coupling between adjacent elements

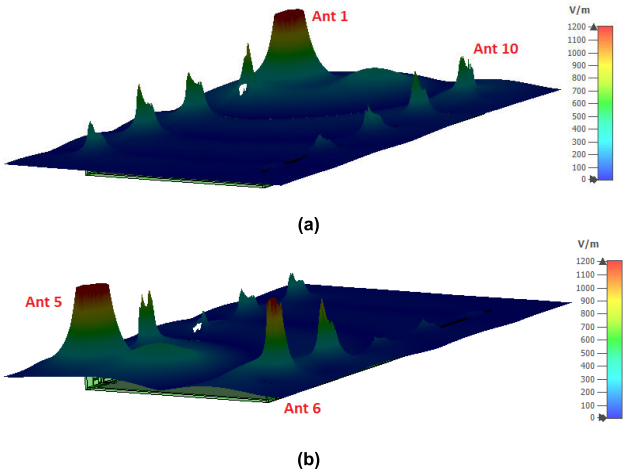

FIGURE 14. Near electric field strength at 3.5 GHz; (a) Antenna 1 is excited, while others are terminated with a 50 Ω load, (b) Antenna 5 is excited, while others are terminated with a 50 Ω load.

is resulted from near field radiation and current flow on the ground plane. Fig. 13 shows that most of the coupling coefficients are below −12 dB, except the mutual coupling coefficient between Ant5 and Ant6 (curve S_{65}) as it peaks around −10 dB. This represents the worst case of coupling although the antennas are located far from each other. The geometry of antenna elements in the proposed array allow us to explain this strange result; by comparing the level of mutual coupling between Ant5-Ant6 and Ant1-Ant10, one can see that they are not the same despite both pairs have the same separation distance. This indicates that the main source of the mutual coupling between Ant5 & Ant6 is the coupling of the fields. Fig. 14 shows that the level of the electric field strength in the near field between Ant1& Ant10 is lower than the case of Ant5 & Ant6 antenna. In conclusion, the predicted results indicate that the proposed antenna array can fully cover the LTE42 frequency band for 5G applications as both the reflection and the isolation parameters are in acceptable ranges.

B. RADIATION PERFORMANCE

Due to large number of antenna elements and the huge number of far-field results, only the simulated and measured normalized polar radiation patterns of Ant 1-Ant 6 in the XY plane are presented. The measurement setup inside an anechoic chamber is attached to the figure. Fig. 15 shows the results of the proposed MIMO antenna at the mid-frequency (3.5 GHz). As shown, a very good agreement is obtained between the simulated and measured far-field radiation patterns. It is also quite noticeable that each antenna has its unique patterns, which interprets the acceptable level of mutual coupling between antennas ports as the patterns peaks are oriented to different directions. Furthermore, Due to the symmetrical placements of the antennas on both edges of the system PCB board, Fig. 15(e) and Fig. 15(f) show that each element in the left-hand PCB edge have complementary

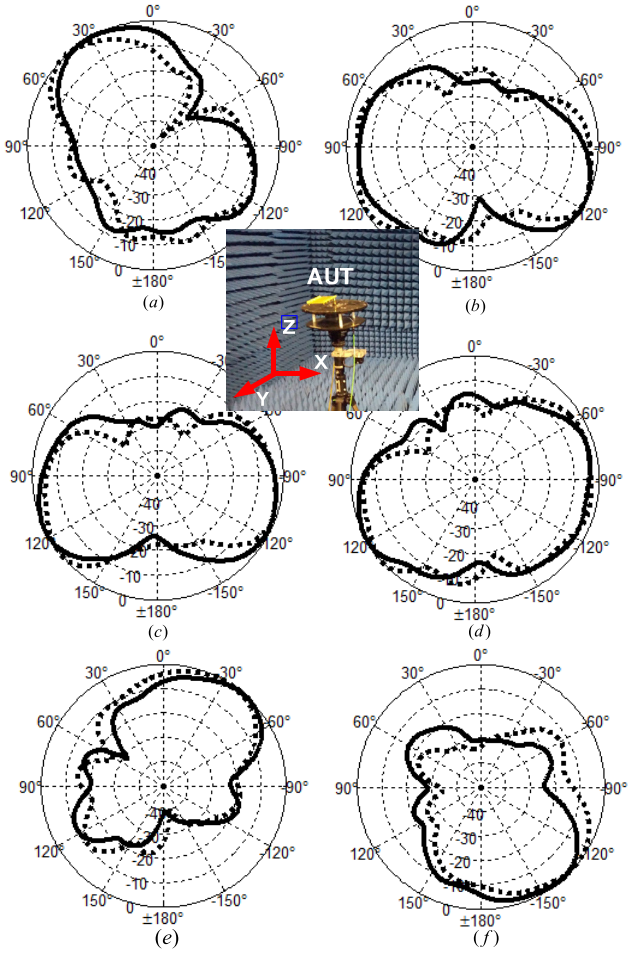

FIGURE 15. Normalized far-field patterns in XY plane; (a) Ant 1, (b) Ant 2, (c) Ant 3, (d) Ant 4, (e) Ant 5 and (f) Ant 6. [Simulated pattern is the solid line and the dotted line for the measured patterns].

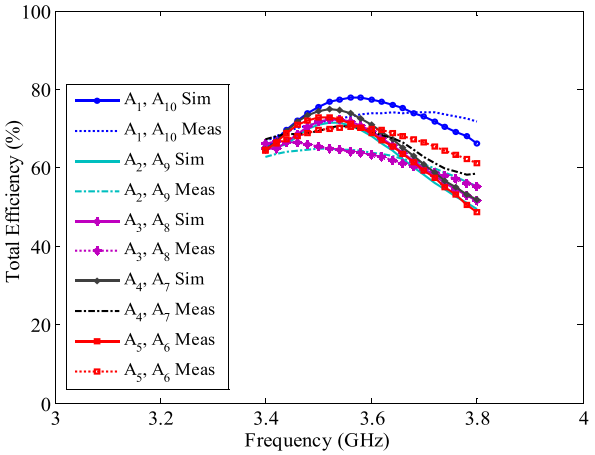

FIGURE 16. Simulated and measured total efficiencies of the proposed antenna.

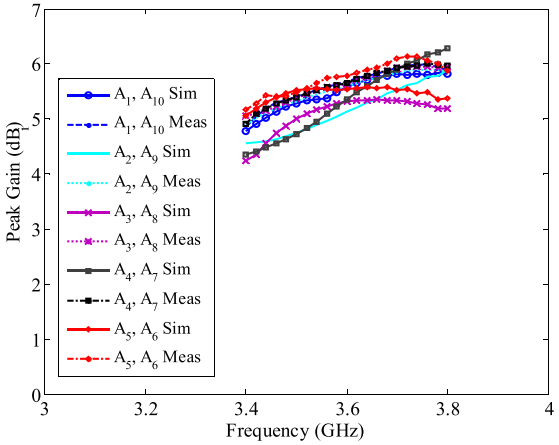

FIGURE 17. Simulated and measured peak antenna gain values.

patterns to its corresponding element on the opposite edge. Therefore, the pattern diversity is achieved which contribute to the low levels of the envelope correlation coefficient (ECC) for MIMO 5G operation.

Fig. 16 shows the simulated and measured total radiation efficiency values of the proposed antenna. The results show that over the entire covered 3.4-3.6 GHz band, the total efficiency values are between 65% and 78%. Therefore, the total efficiency values are acceptable for 5G operation. On the other hand, Fig. 17 shows that both the simulated and the measured peak gains values are in good agreement. The peak gain has a minimum value of 4.2 dBi and a maximum value equals to 5.9 dBi over the frequency band of interest. In comparison to the works reported in the open literature, like the antenna gain results in [3], the proposed loop antenna has highest gain values among the available state-of-the-art designs.

C. MIMO PERFORMANCE

The MIMO performance parameters of the proposed antenna are simulated, measured and evaluated in free space. The envelope correlation coefficient (ECC) results are shown in Fig. 18; they are calculated based on the simulated 3D electric field patterns. For both brevity and symmetry, only the ECC coefficients between consecutive elements located on one PCB side are presented. The results (simulated in Fig. 18(a) and measured in Fig. 18(b)) are in a good agreement. Normally, ECCs are overly less than 0.055 across the entire band of interest. This very low ECC is an obvious result as the maximum gain points of 3D patterns of antenna elements have different directions. This agrees with the criterion of acceptable value for the ECC (<0.5) for MIMO operation [38]. It is worth mentioning that the level of ECC is increased at the band edges as the overlapping between 3D radiation patterns is increased. This can be seen clearly between patterns of Antenna 5 and Antenna 6 (antenna near the corners). Nevertheless, the ECC values are all satisfied the aforementioned ECC MIMO condition.

Furthermore, the ergodic channel capacity (C) is calculated to evaluate the potential MIMO performance of the proposed 10-antenna array prototype. The calculated results were predicted using the following equations (5)-(8) [11], [15].

$$C = E\left\{log_2\left[det\left(I + \frac{SNR}{n}HH^T\right)\right]\right\} \quad (5)$$

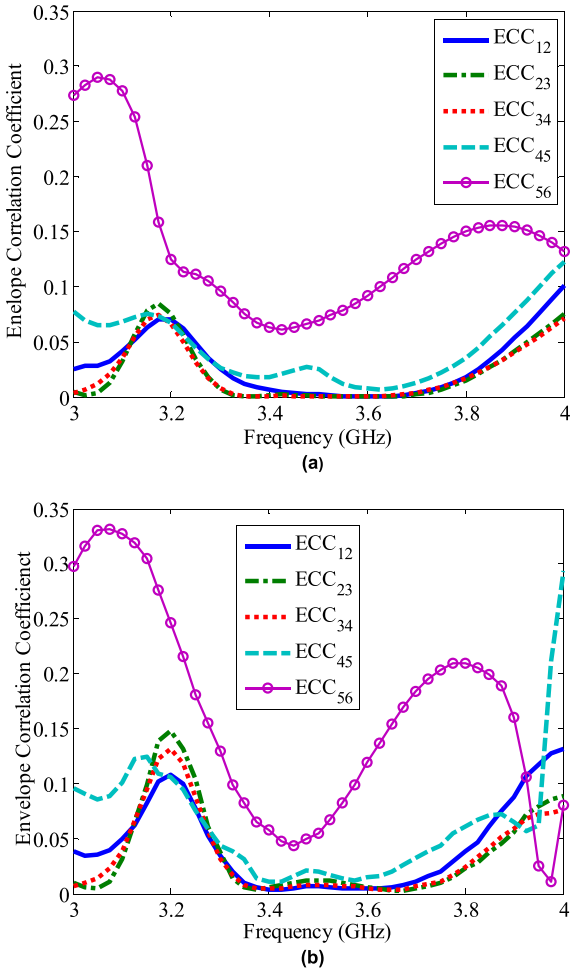

FIGURE 18. Envelope correlation coefficient at 3.5 GHz of the proposed 10-port antenna array; (a) Simulated and (b) Measured.

The channel matric H is calculated using

$$H = \sqrt{\emptyset}_r H_{i,i,d} \sqrt{\emptyset}_t \tag{6}$$

The received and transmit antenna correlation coefficients matrices are defined as follows:

$$\emptyset_r = \sqrt{\eta_{tot,r}} ECC_r \sqrt{\eta_{tot,r}} \tag{7}$$

$$\emptyset_t = \sqrt{\eta_{tot,t}} ECC_t \sqrt{\eta_{tot,t}} \tag{8}$$

The E in (5) represents the expectation with respect to different channel realization. I is a 10 × 10 identity matrix. SNR is the mean signal to noise ratio at the receiving array (proposed prototype). N is the number of transmitting antennas, and $(.)^T$ represents the Hermitian conjugate transpose. During the C calculation it is assumed that the transmitting antennas are uncorrelated ($ECC_T = 0$) and ideal radiators with unity total radiation efficiency. While the prosed 10-element array serves as the receiving antenna array with ECC_r and total efficiency. The $H_{i,i,d}$ is a 10 × 10 matrix, in which its entries are independent identically distributed complex Gaussian random variables.

The calculated C of the proposed 10 × 10 MIMO array is obtained from the measured results by averaging 10,000 independent identically distributed Rayleigh fading channel realization with SNR = 20 dB [12]. Fig. 19 shows the calculated measured C, in which is varies between 52.5-54.3 bps/Hz. The peak C is about 54.3 bps/Hz, which is only 3.2 bps/Hz less than the ideal upper limit of 10 by 10 MIMO system. As compared to the state-of-the-art designs, the proposed 5G antenna solution shows better multiplexing capability than other 10-antenna array designs in [15. 18. 40].

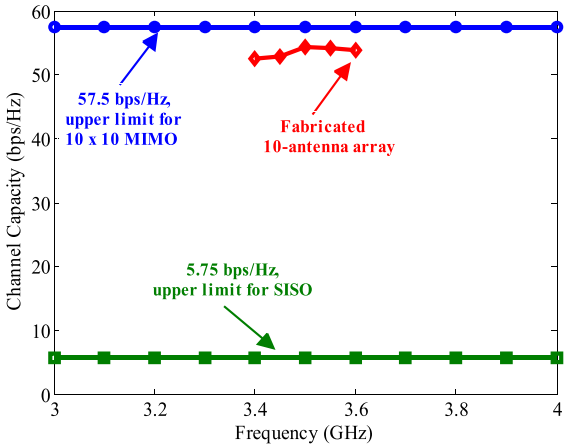

FIGURE 19. Calculated ergodic channel capacities of the proposed 5G antenna array in 10 ×10 MIMO system.

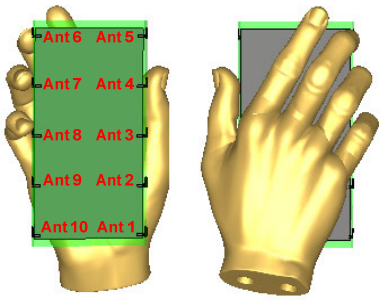

FIGURE 20. Typical single-hand mode (right-hand mode).

D. USER'S HAND EFFECT AND SAR ANALYSIS

The MIMO performance the impact of the user's hand-loading on the performance of the proposed 10-element antenna system is also investigated using CST Microwave Studio [39]. Fig. 20 shows one of the worst-expected scenarios of the user's hand. As depicted in Fig. 21(a), the reflection coefficients of Ant 1, Ant 2, and Ant 4 are slightly shifted to the higher band, but the antennas can still cover the frequency band of interest based-on the −6 dB bandwidth criterion. For some antennas like Ant 3 and Ant 5, the level of matching becomes worse. However, it also covered our band of interest. The isolation levels between all elements are acceptable and further enhanced compared to the free space case, this can be seen from Fig. 21(b).

Fig. 21(c) shows that Ant 1, Ant 2, Ant 3, Ant 4, and Ant 8 have the lowest total efficiencies among array elements.

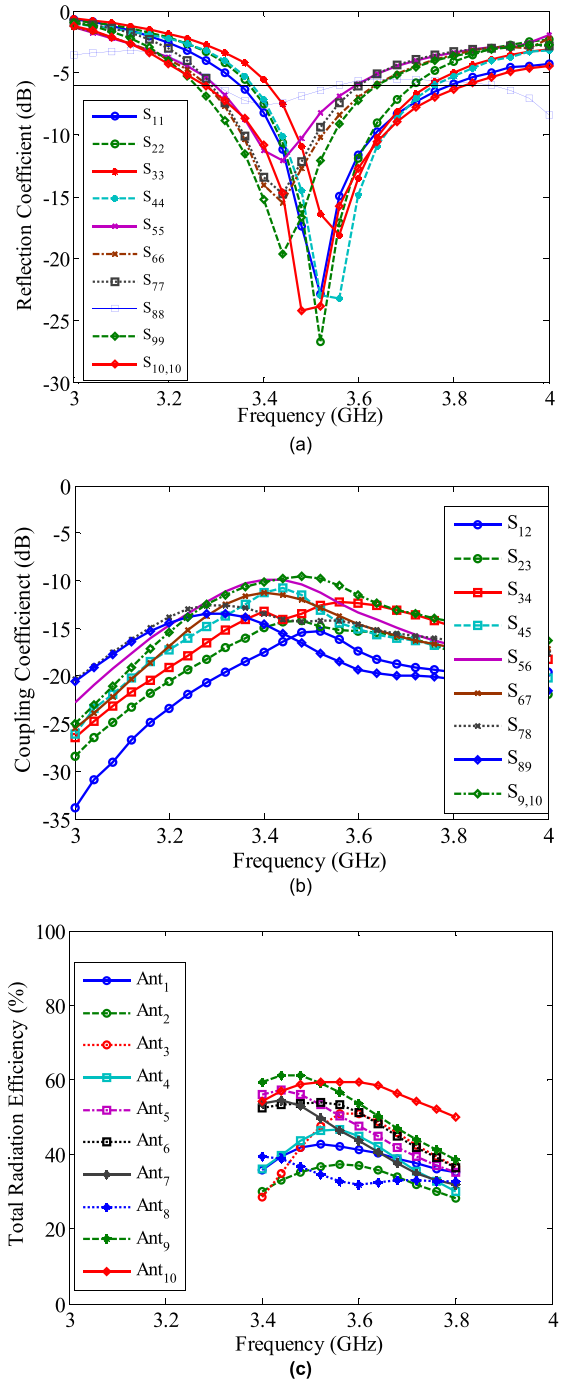

FIGURE 21. User's hand effects on (a) Reflection coefficients, (b) mutual coupling coefficients, and (c) Total radiation efficiencies.

The minimum efficiency is about 30 % at the lower and upper edges of the frequency band of interest. This is because the radiation patterns have a peak in −X and +X direction of element 3 and element 8 as shown from the radiation pattern in azimuth plane in Fig. 15(c). However, compared to the current state-of-the-art, the proposed antenna has the highest level of total efficiency in the presence of the user's hand, knowing that the scenario that is used here is the worst

TABLE 2. Simulated Sar Values for 1 Gram Hand Tissue.

Antenna Element	SA-SAR @ 3.5 GHz
Ant 1	0.63
Ant 2	0.69
Ant 3	0.71
Ant 4	0.76
Ant 5	0.72
Ant 6	0.77
Ant 7	0.79
Ant 8	0.85
Ant 9	0.60
Ant 10	0.54

compared to most of the previous works such as [6], [11], [15], [17], [19]. In contrast, the total efficiency of Ant 5, Ant 6, Ant 7, Ant 9, and Ant 10 are less affected as they are far away from the user's hand. Overall, the proposed MIMO antenna array represents an excellent candidate for 5G mobile communications.

The electromagnetic absorption of a human body has become an important issue for most of hand portable devices. It is evaluated normally by the calculation of the specific absorption rate (SAR). Two different world-wide standards are defined for SAR maximum limits in the USA and the Europe. They are defined as 1.6 W/Kg average 1 g tissue and 2 W/Kg average 10 g tissues, respectively. The transmit power of each element is 14 dBm (25 mW). The stand-alone SAR (SA-SAR) is used to characterize the characterize SAR of the proposed MIMO antenna. This is based on the receive diversity assumption, in which one antenna is normally selected during the receive mode. SA-SAR is calculated when each antenna is excited separately and the other one is terminated with a 50 Ω load. The same mode in Fig. 20 is used in this study. In order to mimic the actual situation and environment, the distance between antenna elements and human tissue is kept less or equal 5 mm. For the purpose of brevity, the achieved results of SA-SAR are all listed in Table 2 . The SAR values are within the industry maximum SAR value limit. Therefore, the proposed MIMO antenna represents an excellent antenna candidate for 5G smartphone applications at 3.5 GHz. Finally, the presented SAR analysis did not compare with the sub-6 GHz 5G antennas state-of-the-art as there is no work report SAR analysis.

V. STATE OF THE ART COMPARISON

In order to highlight the merits of the proposed design compared to previous works, Table 3 shows a comparison between the performances of some recent mobile phone massive MIMO antennas and the proposed antenna. Table 3 shows that the proposed design achieved an excellent ECC level (ECC < 0.055) without using any isolation circuitry. It is also obvious from the table that the proposed design belongs

TABLE 3. Performances Comparison Between the Proposed Antenna and the Current State-of-the-Art.

Ref	Antenna Structure	Impedance Bw (GHz), dB	Mode	Size (W × L × H) [λ^3]	MIMO Order	GRND Clearance	ECC	Isolation (dB)**	η_{tot} (%)
[6]	Loop	3.4-3.6 (-6 dB)	$\lambda/2$	8.96×10^{-5}	8	1	< 0.1	> 11	> 40
[9]	Monopole	2.55-2.65, (-10 dB)	$\lambda/4$	5.04×10^{-5} 10.4×10^{-5}	8	4	< 0.15	> 12	> 53
[3]	Monopole	3.4-3.6 (-6 dB)	$\lambda/4$	6.53×10^{-5}	8	3	< 0.2	> 10**	> 62
[5]	Loop	3.4-3.6 (-10 dB)	$\lambda/2$	13.4×10^{-5}	8	0	< 0.0125	> 20**	> 60
[4]	L-Shaped Monopoles	3.4-3.6 (-10 dB)	$\lambda/4$	19.2×10^{-5}	8	0	< 0.025	> 21**	> 64
[14]	SIW & Open-slot	3.4-3.6 (-6 dB)	$\lambda/4$	277.4×10^{-5}	12	10	< 0.2	> 13	> 55
[7]	Open-slot on bezel	3.4-3.6 (-6 dB)	$\lambda/4$	41.7×10^{-5}	8	1.5	< 0.008	> 12	> 35
[15]	Slot-monopole	3.4-3.6 (-6 dB)	$\lambda/4$	3.85×10^{-5}	10	3	< 0.1	> 10	> 40
[16]	Slot	3.4-3.6 (-10 dB)	$\lambda/4$	8.26×10^{-5}	8	3	<0.05	> 10.5	>62
[17]	Split-loop	3.34-3.84 & 4.66–5.51 (-6 dB)	$\lambda/4$	8.15×10^{-5}	8	0	< .07	> 11**	> 42 & > 40
[19]	U-shaped antenna	3.4-3.6 (-10 dB)	$\lambda/2$	9.91×10^{-5}	8	1	< 0.1	> 17	> 58
[10]	Open slot	3.3-7.1 (-6 dB)	$\lambda/4$	4.73×10^{-5}	8	3	< 0.09	> 10.5	> 47
[11]	Coupled U-shaped strips	3.4-3.6 & 4.8-5.0 (-6 dB)	$\lambda/2$	9.86×10^{-5}	4	1	< 0.14	> 17.5	> 50
[12]	IFA	3.1-6.0 (-6 dB)	$\lambda/4$	12.45×10^{-5}	8	1	< 0.1	> 10	> 41
[18]	IFA	3.3-3.6 & 4.8-5.0, (-6 dB)	$\lambda/4$	7.14×10^{-5}	10	0	< 0.15	> 12	> 45
[20]	Open slots on frame & GRD	3.0-6.0 (-6 dB)	$\lambda/4$	5.72×10^{-5}	8	3	< 0.09	> 11	> 40
[21]	Folded monopole	3.3-3.6 (-6 dB)	$\lambda/4$	28.7×10^{-5}	8	6.6	< 0.2	> 10	> 40
[40]	Open slots	3.6-3.8 & 5.15-5.92 (-6 dB)	$\lambda/4$	6.06×10^{-5}	10	3	< 0.1	> 10	> 52
[*]	**Loop**	**3.4-3.6 (-10 dB)**	$\boldsymbol{\lambda/2}$	$\mathbf{4.96 \times 10^{-5}}$	**10**	**1**	**< 0.055**	**> 10****	**> 65**

**: The resulted antenna array has equally spaced and symmetrical arranged elements over the system PCB.

to an antenna group that not widely utilized as 5G candidate because they work on a half wavelength mode ([6], [5], [11] and [19]), while the rest of reference on the table are among a second antenna group that are designed based on a quarter wavelength structures. These latter types are about 14 recent works (papers). The proposed antenna occupies the smallest footprint size of just 6.5×6 mm^2 with a very small clearance width of only 1 mm to create a total size of $4.96 \times 10^{-5}\lambda^3$. This represents the smallest 5G antenna element in-terms of volumetric size. Moreover, the proposed design has the

highest free space total efficiency (above 65%) among other works.

The proposed antenna has 10 dB worst case ports isolation. However, this level is expected and totally justifiable due to the following reasons: *1)* the resulted antenna array has the highest MIMO order in comparison to the previous works; 10 elements are used in the design while only two sides of the system PCB are used whereas some other works [14], [40] utilize the whole PCB board. *2)* Unlike most reported works [14]–[21], the proposed antenna system has all antenna elements equally spaced and with uniform arrangement. Elements arrangement normally plays important role in minimizing the coupling level.

To meet the current sub-6 5G design trend, both dual-band 10-element and wideband 10-element antennas can be produced by exciting feed resonant frequency and merging it with the next loop mode in the higher bands like n79 band (4400-5000 MHz) or LTE band 46 (5150-5925 MHz). Overall, and a s comprehensive comparison with the listed antennas in the Table 3 , the proposed antenna solution has demonstrated its superiority in-terms of antenna-element size (the smallest), 10-dB impedance bandwidth, the largest radiation efficiency, highest peak gain, and MIMO order.

A. CONCLUSION

A massive MIMO 10-element antenna array operating in the recent sub-6 GHz 5G frequency band is proposed for smartphone applications. The proposed antenna array composed of 10 identical capacitive-fed shorted loop antennas with a spacing of 25 mm between consecutive elements in each smartphone long edges sides. The proposed antenna structure is a compact loop antenna of total area 6×6.5 mm^2 ($0.07\lambda \times 0.0758\lambda$, where λ is the wavelength at 3.5 GHz). The proposed antenna has the smallest literal dimension about $\lambda/13.2$ compared to the current state-of-the-art. The compactness is achieved using both the capacitive feeding method and the inward meandering that forms an internal loop inside. The position and the dimensions of the internal loop are used to tune the resonant frequency and matching level at 3.5 GHz. The measured results show that the 3.5 GHz band (3.4-3.6 GHz) is achieved with impedance matching better than -10 dB, isolation level better than 10 dB, and total efficiency higher than 65%. Moreover, the proposed massive MIMO system shown a good diversity performance with an envelope correlation coefficient below 0.055. Due to the simplicity and compactness of the structure, the proposed 10 element MIMO array represents a promising candidate for low profile 5G massive MIMO antenna in smartphones.

REFERENCES

[1] *User Equipment (UE) Radio Transmission and Reception*, document TS 38.101-1, 3GPP, 2018. [Online]. Available: https://www.3gpp.org/ftp//Specs/archive/38_series/38.101/

[2] L. Wan, Z. Guo, and X. Chen, "Enabling efficient 5G NR and 4G LTE coexistence," *IEEE Wireless Commun.*, vol. 26, no. 1, pp. 6–8, Feb. 2019.

[3] Y.-L. Ban, C. Li, C.-Y.-D. Sim, G. Wu, and K.-L. Wong, "4G/5G multiple antennas for future multi-mode smartphone applications," *IEEE Access*, vol. 4, pp. 2981–2988, 2016.

[4] A. Zhao and Z. Ren, "Multiple-input and multiple-output antenna system with self-isolated antenna element for fifth-generation mobile terminals," *Microw. Opt. Technol. Lett.*, vol. 61, no. 1, pp. 20–27, Jan. 2019.

[5] A. Zhao and Z. Ren, "Size reduction of self-isolated MIMO antenna system for 5G mobile phone applications," *IEEE Antennas Wireless Propag. Lett.*, vol. 18, no. 1, pp. 152–156, Jan. 2019.

[6] K.-L. Wong, C.-Y. Tsai, and J.-Y. Lu, "Two asymmetrically mirrored gap-coupled loop antennas as a compact building block for eight-antenna MIMO array in the future smartphone," *IEEE Trans. Antennas Propag.*, vol. 65, no. 4, pp. 1765–1777, Apr. 2017.

[7] L. Chang, Y. Yu, K. Wei, and H. Wang, "Polarization-orthogonal co-frequency dual antenna pair suitable for 5G MIMO smartphone with metallic bezels," *IEEE Trans. Antennas Propag.*, vol. 67, no. 8, pp. 5212–5220, Aug. 2019.

[8] M. Li, Z. Xu, Y. Ban, C. Sim, and Z. Yu, "Eight-port orthogonally dual-polarised MIMO antennas using loop structures for 5G smartphone," *IET Microw., Antennas Propag.*, vol. 11, no. 12, pp. 1810–1816, Sep. 2017.

[9] M.-Y. Li, Y.-L. Ban, Z.-Q. Xu, C.-Y.-D. Sim, K. Kang, and Z.-F. Yu "Eight-port orthogonally dual-polarized antenna array for 5G smartphone applications," *IEEE Trans. Antennas Propag.*, vol. 64, no. 9, pp. 3820–3830, Sep. 2016.

[10] Q. Cai, Y. Li, X. Zhang, and A. W. Shen, "Wideband MIMO antenna array covering 3.3–7.1 GHz for 5G metal-rimmed smartphone applications," *IEEE Access*, vol. 7, pp. 14270–142084, Sep. 2019.

[11] Z. Ren and A. Zhao, "Dual-band MIMO antenna with compact self-decoupled antenna pairs for 5G mobile applications," *IEEE Access*, vol. 7, pp. 82288–82296, Jul. 2019.

[12] C.-Y.-D. Sim, H.-Y. Liu, and C.-J. Huang, "Wideband MIMO antenna array design for future mobile devices operating in the 5G NR frequency bands n77/n78/n79 and LTE band 46," *IEEE Antennas Wireless Propag. Lett.*, vol. 19, no. 1, pp. 74–78, Jan. 2020.

[13] Y. Li, C.-Y.-D. Sim, Y. Luo, and G. Yang, "12-port 5G massive MIMO antenna array in sub-6 GHz mobile handset for LTE bands 42/43/46 applications," *IEEE Access*, vol. 6, pp. 344–354, 2018.

[14] M.-Y. Li, Y.-L. Ban, Z.-Q. Xu, J. Guo, and Z.-F. Yu, "Tri-polarized 12-antenna MIMO array for future 5G smartphone applications," *IEEE Access*, vol. 6, pp. 6160–6170, Nov. 2018.

[15] K.-L. Wong and J.-Y. Lu, "3.6-GHz 10-antenna array for MIMO operation in the smartphone," *Microw. Opt. Technol. Lett.*, vol. 57, no. 7, pp. 1699–1704, Jul. 2015.

[16] Y. Li, C.-Y.-Y. Sim, Y. Luo, and G. Yang, "High-isolation 3.5 GHz eight-antenna MIMO array using balanced open-slot antenna element for 5G smartphones," *IEEE Trans. Antennas Propag.*, vol. 67, no. 6, pp. 3820–3830, Jun. 2019.

[17] W. Hu, L. Qian, S. Gao, L.-H. Wen, Q. Luo, H. Xu, X. Liu, Y. Liu, and W. Wang, "Dual-band eight-element MIMO array using multi-slot decoupling technique for 5G terminals," *IEEE Access*, vol. 7, pp. 153910–153920, Nov. 2019.

[18] W. Hu, X. Liu, S. Gao, L.-H. Wen, L. Qian, T. Feng, R. Xu, P. Fei, and Y. Liu, "Dual-band ten-element MIMO array based on dual-mode IFAs for 5G terminal applications," *IEEE Access*, vol. 7, pp. 178476–178485, Dec. 2019.

[19] Z. Ren, A. Zhao, and S. Wu, "MIMO antenna with compact decoupled antenna pairs for 5G mobile terminals," *IEEE Antennas Wireless Propag. Lett.*, vol. 18, no. 7, pp. 1367–1371, Jul. 2019.

[20] X. Zhang, Y. Li, W. Wang, and W. Shen, "Ultra-wideband 8-port MIMO antenna array for 5G metal-frame smartphones," *IEEE Access*, vol. 7, pp. 72273–72282, 2019.

[21] J. Guo, L. Cui, C. Li, and B. Sun, "Side-edge frame printed eight-port dual-band antenna array for 5G smartphone applications," *IEEE Trans. Antennas Propag.*, vol. 66, no. 12, pp. 7412–7417, Dec. 2018.

[22] K.-L. Wong, J.-Y. Lu, L.-Y. Chen, W.-Y. Li, and Y.-L. Ban, "8-antenna and 16-antenna arrays using the quad-antenna linear array as a building block for the 3.5-GHz LTE MIMO operation in the smartphone," *Microw. Opt. Technol. Lett.*, vol. 58, no. 1, pp. 174–181, Jan. 2016.

[23] S. S. Alja'afreh, Y. Huang, Q. Xu, L. Xing, and O. A. Saraereh, "MIMO antenna system of a compact 4-element PILA for 4G handset applications," in *Proc. Loughborough Antennas Propag. Conf. (LAPC)*, Loughborough, U.K., Nov. 2016, pp. 1–4.

[24] V. Raghavan, M.-L. Chi, M. A. Tassoudji, O. H. Koymen, and J. Li, "Antenna placement and performance tradeoffs with hand blockage in millimeter wave systems," *IEEE Trans. Commun.*, vol. 67, no. 4, pp. 3082–3096, Apr. 2019.

[25] S. S. Alja'afreh, Y. Huang, L. Xing, Q. Xu, and X. Zhu, "A low-profile and wideband PILA-based antenna for handset diversity applications," *IEEE Antennas Wireless Propag. Lett.*, vol. 14, pp. 923–926, 2015.
[26] S. S. Alja'afreh, Y. Huang, and L. Xing, "A compact, wideband and low profile planar inverted-L antenna," in *Proc. 8th Eur. Conf. Antennas Propag. (EuCAP)*, The Hague, Netherlands, Apr. 2014, pp. 3283–3286.
[27] K.-L. Wong, B.-W. Lin, and B. W.-Y. Li, "Dual-band dual inverted-F/loop antennas as a compact decoupled building block for forming eight 3.5/5.8-GHz MIMO antennas in the future smartphone," *Microw. Opt. Technol. Lett.*, vol. 59, no. 11, pp. 2715–2721, Nov. 2017.
[28] A. Ibraheem and M. Manteghi, "Performance of electrically coupled loop antenna inside human body at different frequency bands," in *Proc. IEEE Antennas Propag. Soc. Int. Symp. (APSURSI)*, Memphis, TN, USA, Jul. 2014, pp. 975–976.
[29] H. Xu, H. Wang, S. Gao, H. Zhou, Y. Huang, Q. Xu, and Y. Cheng, "A compact and low-profile loop antenna with six resonant modes for LTE smartphone," *IEEE Trans. Antennas Propag.*, vol. 64, no. 9, pp. 3743–3751, Sep. 2016.
[30] E. Danial, "Novel approaches to the design of phased array antennas," Ph.D. dissertation, Dept. Elect. Comput. Eng. Division, Univ. Michigan, Ann Arbor, Michigan, 2011.
[31] S. S. Alja'afreh, Y. Huang, and L. Xing, "A novel, low profile and wideband PIFA antenna with polarization and pattern diversities," *IET Microw., Antennas Propag.*, vol. 10, no. 2, pp. 152–161, Jan. 2016.
[32] M. H. Alshamaileh, S. S. Alja'afreh, and E. Almajali, "Nona-band, hybrid antenna for metal-rimmed smartphone applications," *IET Microw., Antennas Propag.*, vol. 13, no. 14, pp. 2439–2448, Nov. 2019.
[33] A. Pyattaev, D. Solomitckii, and A. Ometov, "3D folded loop UAV antenna design," in *Proc. Int. Conf. Wired/Wireless Internet Commun.* Cham, Switzerland: Springer, 2018, pp. 269–281.
[34] D. M. Pozar, *Microwave Engineering*. Hoboken, NJ, USA: Wiley, 2012.
[35] Z. Qamar, U. Naeem, S. A. Khan, M. Chongcheawchamnan, and M. F. Shafique, "Mutual coupling reduction for high-performance densely packed patch antenna arrays on finite substrate," *IEEE Trans. Antennas Propag.*, vol. 64, no. 5, pp. 1653–1660, May 2016.
[36] H. Chreim, R. Chantalat, M. Thevenot, U. Naeem, S. Bila, T. Monediere, B. Palacin, Y. Cailloce, G. Caille, and P. De Maagt, "An enhanced *Ka*-band reflector focal-plane array using a multifeed EBG structure," *IEEE Antennas Wireless Propag. Lett.*, vol. 9, pp. 1152–1156, 2010.
[37] C. K. Alexander and M. N. O. Sadiku, *Fundamentals of Electric Circuits*. Boston, MA, USA: McGraw-Hill, 2007.
[38] S. S. Alja'afreh, "MIMO antennas for mobile phone applications," Ph.D. dissertation, Dept. Elect. Electron. Eng., Univ. Liverpool, Liverpool, U.K., 2015.
[39] *CST*. Accessed: Oct. 20, 2020. [Online]. Available: https://www.cst.com
[40] Y. Li and G. Yang, "Dual-mode and triple-band 10-antenna handset array and its multiple-input multiple-output performance evaluation in 5G," *Int. J. RF Microw. Comput.-Aided Eng.*, vol. 29, Dec. 2018, Art. no. e21538.

SAQER S. ALJA'AFREH received the B.Sc. and M.Sc. degrees in engineering from the Faculty of Engineering, Mutah University, Al-Karak, Jordan, in 2004 and 2007, respectively, and the Ph.D. degree in electrical engineering from the University of Liverpool, Liverpool, U.K., in October 2015. He was a Field Engineer in Amman, Jordan, from 2008 to 2009, and also a Lecturer with the Department of Electrical Engineering, Mutah University, from 2009 to 2012, where he was the Head from 2017 to 2018 and has been an Assistant Professor in electrical engineering since November 2015. He has published more than 50-refereed articles in leading journals and conference proceedings. His current research interests include MIMO and diversity antennas, 4G/5G antennas, dielectric resonator antennas, planar antennas, and microwave circuits. Recently, he received a 50 000 GBP Royal Academy grant for the development of an undergraduate industry related mobile communications course in communications engineering curriculum. In summer 2018, he received the Guest Visit Award of the Doutche Forschungsgemeinschaft German Research Foundation.

BAYAN ALTARAWNEH received the B.Sc. and M.Sc. degrees in engineering from the Faculty of Engineering, Mutah University, Al-Karak, Jordan, in 2011 and 2019, respectively.

MALLAK H. ALSHAMAILEH received the B.Sc. and M.Sc. degrees in engineering from the Faculty of Engineering, Mutah University, Al-Karak, Jordan, in 2016 and 2018, respectively. Her current research interests include 4G/5G antennas and multiband antennas.

E'QAB R. ALMAJALI received the B.Sc. degree (Hons.) from Mutah University, Jordan, in 2002, and the M.A.Sc. and Ph.D. degrees (Hons.) from the University of Ottawa, Ottawa, ON, Canada, in 2010 and 2014, respectively, all in electrical engineering.

He was a Postdoctoral Fellow with the Electronics Department, Carleton University, Canada. Since August 2018, he has been an Assistant Professor with the Electrical Engineering Department, University of Sharjah. He has authored more than 35 technical publications and a book chapter (Artech, 2013) on reflectarray antennas. His current research interests include frequency selective surfaces, millimeter-wave MIMO antennas and integrated 4G/5G antennas for wireless handsets, and transmitarrays and low profile holographi antennas.

Dr. E'qab received the prestigious Canadian National Science and Engineering Research Council (NSERC) Postdoctoral Fellowship, in 2014, for his research excellence and also received the NSERC-PGS Scholarship during his Ph.D. studies, in 2012.

RIFAQAT HUSSAIN received the B.Sc. degree (Hons.) in electrical engineering from the University of Engineering and Technology, Peshawar, Pakistan, in 2003, the M.S. degree in systems engineering from PIEAS, Pakistan, in 2005, and the Ph.D. degree in electrical engineering from the King Fahd University of Petroleum and Minerals (KFUPM), Dhahran, Saudi Arabia, in January 2015. He served as a Senior Engineer for Public Sector Research and Development Organization, Pakistan, from 2005 to 2011. He is currently a Faculty Member and associated with the Antenna and Microwave Structure Desing Lab (MASDL), King Fahd University of Petroleum & Minerals. His current research interests include reconfigurable antennas, 4G/5G integrated antenna designs, CubeSat antenna, the IoT, and 5G enabled antenna design.

MOHAMMAD S. SHARAWI (Senior Member, IEEE) received the Ph.D. degree from Oakland University, MI, USA, in 2006. From 2009 to 2018, he was with the King Fahd University of Petroleum and Minerals (KFUPM), Saudi Arabia. He founded and directed the Antennas and Microwave Structure Design Laboratory (AMSDL), KFUPM. He has been a Visiting Professor with the Intelligent Radio (iRadio) Laboratory, Electrical Engineering Department, University of Calgary, AB, Canada, since Summer-Fall of 2014. In summer of 2013, he was a Visiting Research Professor with Oakland University. He is currently a Professor of electrical engineering with Polytechnique Montréal, QC, Canada, where he is also a member of the Poly-Grames Research Center. He has more than 300 articles published in refereed journals and international conferences, 10 book chapters, one single authored book entitled *Printed MIMO Antenna Engineering* (Artech House, 2014), and the Lead Author of the recent book *Design and Applications of Active Integrated Antennas* (Artech House, 2018). He has 25 issued and 12 pending patents in the U.S. Patent Office. His research interests include multiband printed multiple input-multiple-output (MIMO) antenna systems, reconfigurable and active integrated antennas, applied electromagnetics, millimeter-wave MIMO antennas, and integrated 4G/5G antennas for wireless handsets and access points.

Dr. Sharawi served on the technical and organizational program committees for several international conferences such as EuCAP, APS, IMWS-5G, APCAP, iWAT, and among many others. He is serving as the Associate Editor for the IEEE Antennas and Wireless Propagation Letters (AWPL) and *IET Microwaves, Antennas and Propagation* (MAP), and an Area Editor for *Microwave and Optical Technology Letters* (MOP) (Wiley). He is the Specialty Editor of the newly launched *Frontiers Journal on Communications and Networking* and the System and Test-Bed design section.

LEI XING (Member, IEEE) is currently a Lecturer with the College of Electronic and Information Engineering, Nanjing University of Aeronautics and Astronautics, China. Her research interests include liquid antennas and antenna measurements, hand-portable antennas, and reconfigurable antennas.

QIAN XU (Member, IEEE) is currently an Associate Professor with the College of Electronic and Information Engineering, Nanjing University of Aeronautics and Astronautics, China. His research interests include statistical electromagnetics and reverberation chambers.